ISSN 0021-3640, JETP Letters, 2022, Vol. 115, No. 10, pp. 602–607. © The Author(s), 2022. This article is an open access publication, corrected publication 2022.
Russian Text © The Author(s), 2022, published in Pis'ma v Zhurnal Eksperimental'noi i Teoreticheskoi Fiziki, 2022, Vol. 115, No. 10, pp. 636–641.

PLASMA, HYDRO- AND GAS DYNAMICS

Channeling of Auroral Kilometric Radiation During Geomagnetic Disturbances

M. M. Mogilevsky[a, *], D. V. Chugunin[a], A. A. Chernyshov[a], V. I. Kolpak[a, b, c], I. L. Moiseenko[a], Y. Kasahara[d], and Y. Miyoshi[e]

[a] *Space Research Institute, Russian Academy of Sciences, Moscow, 117997 Russia*
[b] *National Research University Higher School of Economics, Moscow, 101000 Russia*
[c] *Pushkov Institute of Terrestrial Magnetism, Ionosphere, and Radio Wave Propagation, Russian Academy of Sciences, Troitsk, Moscow, 108840 Russia*
[d] *Kanazawa University, 920-1192 Kanazawa, Japan*
[e] *Nagoya University, 464-8601 Nagoya, Japan*
**e-mail: mogilevsky2012@gmail.com*

Received April 19, 2022; revised April 22, 2022; accepted April 22, 2022

The electromagnetic fields measured on the ERG satellite are presented and their comparative analysis with measurements on the WIND satellite is carried out. The possibility of capturing auroral kilometric radiation (AKR) into plasma channels, which was first discovered on the ISEE satellite, has been confirmed. Plasma inhomogeneities, formed with an increase in geomagnetic activity, are extended along the magnetic field and form channels along which the radiation propagates. The trapped radiation spectrum is distorted because of the relative position of the source and channel at low frequencies. The distortion of the AKR spectrum at high frequencies is related to the frequency dependence of propagation conditions in the channel. Asymmetry of the processes of formation of plasma channels and AKR sources in the northern and southern auroral regions is found.

DOI: 10.1134/S0021364022600707

1. The propagation of low-frequency electromagnetic waves in a plasma with inhomogeneities was studied in detail [1, 2]. For the passage of an electromagnetic pulse caused by a lightning discharge, it is necessary to "screw" the wave vector in the equator region of the conjugated hemisphere, which can be realized when a signal propagates in plasma channels, the so-called ducts—plasma inhomogeneities, extended along the magnetic field. Such ducts are formed as a result of elongation of ionospheric inhomogeneities along the field, and radiation is trapped in the upper ionosphere. Similarly, the propagation of signals from ground-based low-frequency transmitters from one hemisphere to another occurs [3, 4]. Low-frequency radiation propagation in plasma channels with increased ($\Delta N/N > 0$) and reduced ($\Delta N/N < 0$) plasma densities were theoretically considered in [5, 6]. Another mechanism of duct formation was reported in [7]. Fast measurements of the plasma density showed that, during geomagnetic disturbances, the plasmasphere approaches the Earth and, near the equatorial plane, plasma clots separate from it and then extend along the magnetic field. The resulting plasma channels trap the radiation generated near the equatorial region, for example, plasmaspheric hiss, which penetrates into the ionosphere through these channels.

In 1982, it was discovered on the ISEE-1 satellite that auroral kilometric radiation (AKR) can also be trapped into plasma channels and ducts and propagate through these channels from auroral regions to the inner regions of the magnetosphere, the plasmasphere [8]. Unlike very low frequency radiation, AKR is trapped only in channels with a reduced density ($\Delta N/N < 0$) and propagates in them over considerable distances.

2. In this paper, the results of measurements of AKR trapped into a plasma channel and the propagation of this radiation in such a channel are considered. For this purpose, the results of measurements on the ERG (Arase) satellite, which was launched on December 20, 2016, into an elliptical orbit with an apogee of ~32 110 km (about six Earth radii), a perigee of ~460 km, an orbit inclination of 31°, and a rotation period of 8 s [9], were used. The observations used in this paper were made with a High Frequency Analyzer (HFA) [10], which is one of the instruments used in the Plasma Wave Experiment (PWE) [11]. The HFA calculates electric field spectra in the frequency range of 2 kHz–10 MHz for two components perpendicular

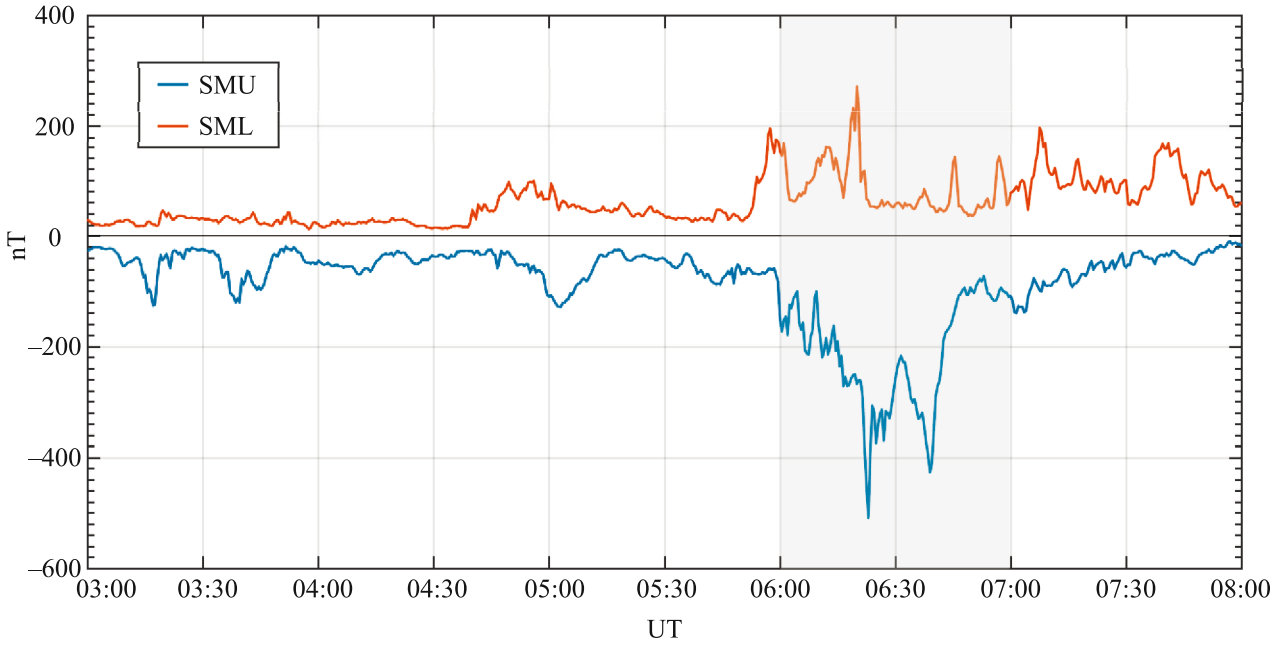

Fig. 1. (Color online) Geomagnetic activity indices SMU and SML. The time of radiation detection on the ERG satellite is highlighted in gray.

to the satellite rotation axis, which is directed to the Sun. The time resolution is 8 s and the frequency resolution is $-\Delta f/f < 2.5\%$. The data of the ERG satellite and features of its orbit were previously used to study the AKR and continuum radiation near the equatorial region [12–14].

To reveal the features of the radiation spectrum trapped into the plasma waveguide, the measurements onboard the Arase satellite were compared with the observations on the WIND satellite. The WIND satellite was launched on November 1, 1994, to the L1 Lagrange point and is operating safely at the present time. In this work, measurements of the electric field in the Waves experiment in the frequency range of 20–1040 kHz (RAD1) [15] were used.

3. Figure 1 demonstrates the SMU and SML geomagnetic activity indices in auroral regions [16]. The time of detection of radiations on the ERG satellite is marked with a gray background. For 6 h before the start of measurements, the geomagnetic situation was calm, and a small geomagnetic disturbance, up to 500 nT, began at 08:50 UT, the active part of which lasted until 10:30 UT, and then weakened. The presence of the small disturbance is confirmed by measurements of the magnetic field in the solar wind, which caused the substorm (see the supplementary material).

4. The electric field measured on December 19, 2018, on the ERG (Arase) satellite is demonstrated in Fig. 2. During the measurements, the satellite was located mainly in the Southern Hemisphere ($Z_{sm} < 0$, where Z_{sm} is the Z coordinate in the solar-magnetic coordinate system) and moved along the ascending part of the orbit away from the Earth: the satellite at 09:00 UT was at the boundary of the plasmasphere and at 11:00 UT was near the apogee. The top panel of Fig. 2 demonstrates the dynamic spectrogram of the electric field amplitude in the frequency range of 20–800 kHz. According to this figure, AKR bursts are observed in the frequency range of 200–400 kHz with an average characteristic interval of about 6 min until 10:10 UT and then more often, with a characteristic interval of 2–3 min. A narrowband signal at a frequency decreasing from ~200 to ~100 kHz is a field oscillation at the upper hybrid resonance (UHR) frequency, $\omega_{UHR} = (\omega_{pe}^2 + \omega_{Be}^2)^{1/2}$, where ω_{pe} and ω_{Be} are the plasma frequency and the gyrofrequency of the electrons, respectively. Variations of the upper hybrid resonance frequency ($\Delta\omega_{UHR}/\omega_{UHR} \sim 0.5$) are associated with changes in the plasma density, since the magnetic field in the observation interval changes smoothly from ~460 to ~120 nT (which corresponds to a cyclotron frequency of 13–4.5 kHz) and cannot be responsible for such significant changes in the hybrid frequency. Horizontal stripes on the spectrogram at a frequency of 110 kHz and its harmonics are onboard noise.

Auroral kilometric radiation bursts are recorded synchronously with a decrease in the upper hybrid resonance frequency, which indicates the propagation of the radiation inside channels with a reduced plasma density.

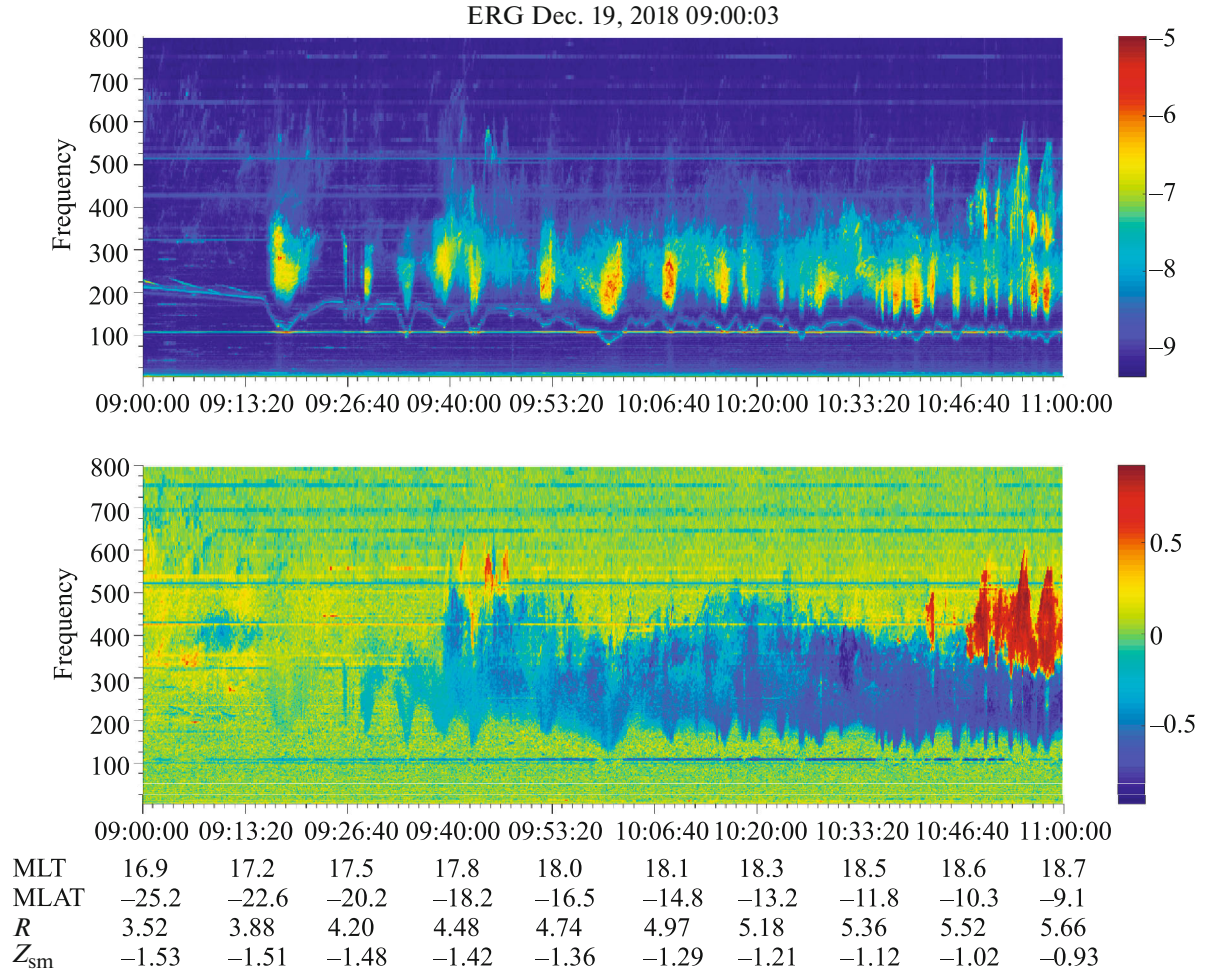

Fig. 2. (Color online) (Upper panel) Dynamic spectrogram of the electric field of radiation recorded in the interval of 09–11 UT on December 19, 2018. (Lower panel) Spectrogram of the polarization coefficient.

The bottom panel of Fig. 2 demonstrates the spectrogram of the radiation polarization coefficient calculated on board with respect to the satellite rotation axis [9] using two mutually perpendicular components of the electric field E_u and E_v. The projections of the left and right components on the UV plane determined by the components E_u and E_v are expressed in terms of the complex Fourier coefficients $\widetilde{E_u}$ and $\widetilde{E_v}$ of E_u and E_v, respectively, as

$$|\widetilde{E_L}|^2 = \widetilde{E_u} + \widetilde{E_v}\exp[-(\pi/2)i]^2/2 = (|\widetilde{E_u}|^2 + |\widetilde{E_v}|^2)/2 - \mathrm{Im}\widetilde{E_u}\widetilde{E_v}^*, \quad (1)$$

$$|\widetilde{E_R}|^2 = \widetilde{E_u} + \widetilde{E_v}\exp[+(\pi/2)i]^2/2 = (|\widetilde{E_u}|^2 + |\widetilde{E_v}|^2)/2 + \mathrm{Im}\widetilde{E_u}\widetilde{E_v}^*, \quad (2)$$

where the asterisk means complex conjugation and Im denotes the imaginary part.

After averaging over one rotation of the satellite, 8 s, the polarization coefficient is determined as

$$K(f) = (\langle|\widetilde{E_R}|^2\rangle - \langle|\widetilde{E_L}|^2\rangle)/(\langle|\widetilde{E_R}|^2\rangle + \langle|\widetilde{E_L}|^2\rangle). \quad (3)$$

Since the rotation axis of the satellite is directed toward the Sun, the polarization coefficient depends not only on the radiation polarization but also on the relative position of the radiation source and the satellite. The AKR burst at 09:17 UT in Fig. 2 is almost linearly polarized ($K(f) = 0$), and then, as the satellite moves to the night side of the magnetosphere, the polarization of AKR bursts changes (decreases), and at 11:00 UT, it reaches 0.8, which indicates the right polarization of radiation from a source located in the Northern Hemisphere.

The relative position of the ERG and WIND satellites, and the AKR source demonstrated in Fig. S2 in the supplementary material allows comparison of the AKR signals received on two satellites, as demonstrated in Fig. S3 in the supplementary material.

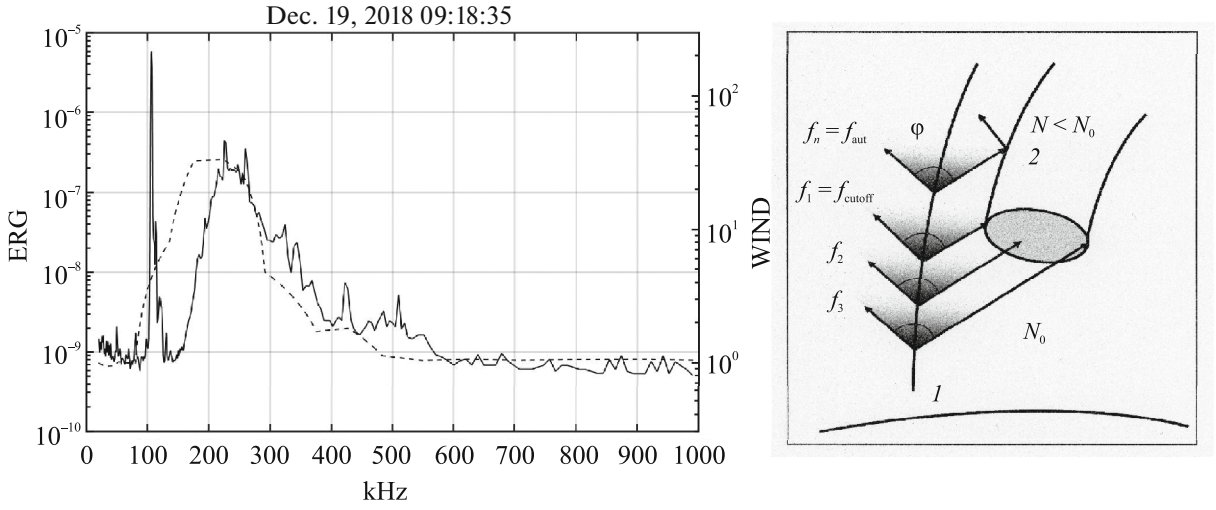

Fig. 3. (Left part) Auroral kilometric radiation (AKR) spectra simultaneously recorded on the (solid line) ERG and (dashed line) WIND satellites. The spike at 100–130 kHz is the upper hybrid frequency. (Right part) Schematic illustration explaining the cutoff of the spectrum components at low frequencies when radiation is trapped into the channel: (*1*) magnetic field line on which the AKR source is located, (*2*) plasma channel with reduced density, and (φ) opening angle of the AKR cone at the source output. The limited opening of the radiation cone and channel dimensions limit the entry of frequencies below f_1 into the channel, the source of which is located above. At frequency f_2, the signal enters the channel partially, and at frequency f_3 and above, it enters completely.

Figure 3 demonstrates the AKR radiation spectra recorded simultaneously on two satellites at 09:18:35 UT. Part of the radiation at low frequencies (100–200 kHz) is observed on the WIND satellite, but is not visible on the ERG satellite. Such a cutoff of the low-frequency part of the spectrum is associated with restrictions on radiation trapped into the channel and is determined by the ratio of the channel dimensions, the opening angle of the radiation cone, and the altitude dependence of the AKR generation frequency [17, 18]. Since the AKR is generated at the local electron gyrofrequency, which depends on the altitude, the higher frequency radiation generated at a lower altitude enters the channel completely. Radiation coming from high altitudes partially enters the channel, while frequencies above f_1 (in Fig. 3) do not enter the channel at all, since the radiation cone and channel dimensions limit the trapping conditions.

The decrease in the spectrum at high frequencies is due to the conditions of radiation reflection from the walls of the plasma channel. Since the transverse size of the channel is much larger than the radiation wavelength, it is possible to use the geometrical optics approximation for the reflection coefficient from an inhomogeneous plasma [19]

$$r = \frac{N_1 \cos\varphi_1 - N_2 \cos\varphi_2}{N_1 \cos\varphi_1 + N_2 \cos\varphi_2}, \qquad (4)$$

where N_1 and N_2 are the refractive indices inside and outside the channel, respectively, and φ_1 and φ_2 are the angles of incidence and refraction, respectively.

Since $N^2 \sim (1 - \omega_0^2/\omega^2)$ [20], as the radiation frequency increases, the refractive index approaches 1 and the reflection coefficient decreases. The total signal power in the opposite hemisphere is formed by multiple reflections ($\sum r = r^n$, where n is the number of reflections, and for a specific example, n can reach several tens), which leads to a faster decrease in the signal with increasing frequency.

An example of the simultaneous capture of radiation from two sources, one in the Northern Hemisphere and the other in the Southern Hemisphere, into a channel is demonstrated in Fig. 4.

The first maximum in the AKR spectrum is observed at a frequency of 190 kHz, which corresponds to a generation altitude of ~6900 km. The second maximum is observed at a frequency of 350 kHz and the AKR generation altitude is ~4300 km. When passing from the first maximum to the second, the radiation polarization changes from negative to positive. This change in the polarization indicates that radiation from northern sources dominates at low frequencies, while radiation from southern sources becomes dominant at higher frequencies above ~310 kHz. The difference between the "northern" and "southern" maxima in the AKR spectrum can be due to different channel formation rates in the Northern Hemisphere and Southern Hemisphere; as a result, the ends of the channels are at different altitudes. Another explanation for the difference in the frequency of maxima in the spectrum may be different positions of the field line of the AKR source with

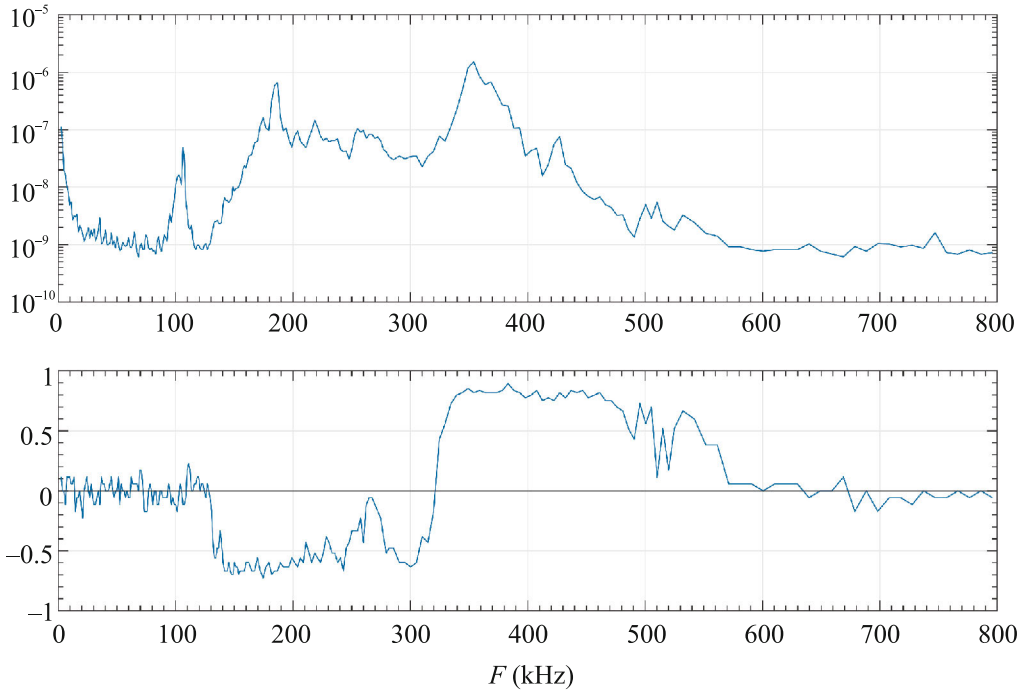

Fig. 4. (Color online) Characteristics of the AKR measured at 10:49:55 UT on December 19, 2018. (Upper panel) Signal amplitude spectrum in the frequency range of 2 kHz–1 MHz. (Lower panel) Polarization coefficient spectrum. Negative and positive values of this coefficient correspond to sources located in the Northern Hemisphere and Southern Hemisphere, respectively. The spike at 100 kHz in the amplitude spectrum is the upper hybrid resonance frequency.

respect to the channel entrance. In this case, the southern field line of the source should be located closer to the pole and further from the channel, while the northern one should be closer to the equator and, accordingly, closer to the channel.

5. The analysis of AKR measurements on the ERG satellite has provided the following conclusions.

—These measurements have confirmed that AKR can be trapped into a channel formed by plasma inhomogeneities at the outer boundary of the plasmasphere, as was previously observed on the ISEE-1 satellite.

—Plasma channels can be formed at low geomagnetic activity, as well as AKR.

—When AKR is trapped into the plasma channel, the radiation spectrum changes: the radiation intensity increases quite rapidly at low frequencies (~1 $mV^2/(m^2\ Hz)$) and decreases quite slowly at high frequencies (–(0.15 – 0.25) $mV^2/(m^2\ Hz)$).

—The processes of formation of plasma channels and AKR sources in the northern and southern auroral regions are asymmetric.

Hence, the relative position of the magnetic field axis can be determined from the measured spectrum of cyclotron radiation from planets and exoplanets: broadband radiation with a “rectangular” spectrum should be detected from high-latitude regions of the magnetosphere, whereas the radiation spectrum from near the equatorial region is distorted, resulting in a “triangular” spectrum.

ACKNOWLEDGMENTS

The ERG (Arase) satellite data were obtained from the ERG Science Center https://ergsc.isee.nagoya-u.ac.jp [10]; the study analyzes data from the PWE HFA-L2 v01.01 instrument [11]. The WIND satellite data are available on the website https://cdaweb.gsfc.nasa.gov/pub/data/wind/waves/wav_h1/. We are grateful to the organizations and national agencies that are members of SuperMAG [http://supermag.jhuapl.edu/info] for providing data on geomagnetic activity indices.

FUNDING

A. Chernyshov and V. Kolpak acknowledge the support of the Foundation for the Advancement of Theoretical Physics and Mathematics BASIS. M. Mogilevsky acknowledge the support of the Ministry of Science and Higher Education of the Russian Federation, project no. 075-15-2020-780 (N13.1902.21.0039).

CONFLICT OF INTEREST

The authors declare that they have no conflicts of interest.

SUPPLEMENTARY INFORMATION

The online version contains supplementary material available at https://doi.org/10.1134/S0021364022600707.

REFERENCES

1. R. A. Helliwell, *Whistlers and Related Ionospheric Phenomena* (Stanford Univ. Press, Stanford, 1965).
2. O. A. Molchanov, *Low-Frequency Waves and Induced Radiation in Near-Earth Plasma* (Nauka, Moscow, 1985) [in Russian].
3. Ya. I. Likhter, O. A. Molchanov, and V. M. Chmyrev, JETP Lett. **14**, 325 (1971).
4. A. A. Petrukovich, M. M. Mogilevsky, A. A. Chernyshov, and D. R. Shklyar, Phys. Usp. **58**, 606 (2015).
5. V. I. Karpman and R. N. Kaufman, Geomagn. Aeron. **23**, 451 (1983).
6. V. I. Karpman and R. N. Kaufman, Geomagn. Aeron. **23**, 791 (1983).
7. C. Beghin, J. F. Karczewski, B. Poirier, R. Debrie, and N. Massevitch, Ann. Geophys. **38**, 615 (1982).
8. W. Calvert, Geophys. Res. Lett. **9**, 56 (1982).
9. Y. Miyoshi, I. Shinohara, T. Takashima, et al., Earth, Planets Space **70**, 101 (2018).
10. A. Kumamoto, F. Tsuchiya, Y. Kasahara, et al., Earth, Planets Space **70**, 82 (2018).
11. Y. Kasahara, Y. Kasaba, H. Kojima, et al., Earth, Planets Space **70**, 86 (2018).
12. M. M. Mogilevsky, D. V. Chugunin, A. A. Chernyshov, T. V. Romantsova, I. L. Moiseenko, A. Kumamoto, and J. Kasakhara, JETP Lett. **114**, 23 (2021).
13. V. I. Kolpak, M. M. Mogilevsky, D. V. Chugunin, A. A. Chernyshov, I. L. Moiseenko, A. Kumamoto, F. Tsuchiya, E. Kasakhara, M. Shoii, E. Mieshi, and I. Shinokhara, Soln.-Zemn. Fiz. **7** (1), 13 (2021).
14. A. A. Chernyshov, M. M. Mogilevsky, D. V. Chugunin, and V. I. Kolpak, Bull. Russ. Acad. Sci.: Phys. **86**, 295 (2022).
15. R. Harten and K. Clark, Space Sci. Rev. **71**, 23 (1995).
16. P. T. Newell and J. W. Gjerloev, J. Geophys. Res. (Space Phys.) **116**, A12211 (2011).
17. M. M. Mogilevsky, T. V. Romantsova, J. Hanasz, T. M. Burinskaya, and R. Shraiber, JETP Lett. **86**, 709 (2007).
18. A. A. Chernyshov, D. V. Chugunin, and M. M. Mogilevsky, JETP Lett. **115**, 23 (2022).
19. G. S. Landsberg, *Optics,* 5th ed. (Nauka, Moscow, 1976) [in Russian].
20. V. L. Ginzburg, *Propagation of Electromagnetic Waves in Plasma* (Nauka, Moscow, 1967; Addison-Wesley, London, 1970).

Translated by R. Bando